Intense THz source based on laser modulator and bunch compressor with electron beam ranging from 35 to 50 MeV

K. Kan†

SLAC National Accelerator Laboratory
Menlo Park, California 94025, USA
The Institute of Scientific and Industrial Research (ISIR), Osaka University,8-1Mihogaoka, Ibaraki, Osaka 567-0047, Japan
†E-mail: koichi@slac.stanford.edu

Z. Huang‡ and G. Marcus

SLAC National Accelerator Laboratory
Menlo Park, California 94025, USA
‡E-mail: zrh@slac.stanford.edu

Z. Zhang

Department of Engineering Physics, Tsinghua University
Beijing 100084, China

Simulation studies on terahertz (THz) free electron laser (FEL) using a laser modulator and a bunch compressor are reported. The laser modulator for slice energy spread modulation and the momentum compaction factor in the bunch compressor were optimized for higher bunching factor in THz range. Finally, the density-modulated electron beam after the bunch compressor was used for coherent undulator radiation and FEL amplification. In our simulations, electron beam with bunch length of 10 ps, bunch charge of 1 nC, bunching factor of ~0.3, and energy ranging from 35 to 50 MeV was discussed for the THz generation. Tunable frequency ranging from 2 to 10 THz and pulse energy of the order on 100 μJ will be indicated.

Keywords: Terahertz (THz) radiation, Laser modulator, Coherent undulator radiation.

1. Introduction

Picosecond or femtosecond electron beams are useful for generation of electromagnetic waves. High-brightness electron beams are used for light sources with wavelengths such as X-ray [1-4], ultraviolet [5], and terahertz (THz) (mid-infrared) [6] lights with free electron lasers (FELs). Generation and control of high-brightness electron beams are also studied because the quality of light source depends on the electron beam characteristics. High-power THz sources using lasers and electron beams in the THz gap between radio waves and infrared light attract many interests from viewpoints of applications and researches [7].

Optical rectification induced by lasers is widely used for high-power THz sources, and THz pulse energies ranging from 1 to 680 μJ [8-11] was reported. In optical rectification, laser pulses with energy of the order on 1 mJ are converted to THz pulses in lithium niobate [8,9] or organic crystal [10,11]. Softening amino acid for structural control [8] and impact ionization of nonlinear effect [9] were reported using intense THz

pulses. THz photon energy corresponds to 24 meV at 10 THz, however, detection using silicon-based camera which has band gap energy of 1.1 eV was performed due to nonlinear effect with intense THz pulses at ~10 THz [11]. Thus, THz pulses with energy ranging from 1 μJ to 1 mJ and electric field of the order on 1 MV/m could be powerful tools for the investigation of such nonlinear effects and applications.

For high-power THz sources using electron beam, THz pulse from coherent transition radiation using a metal interface was detected by a silicon photodetector for THz pulse energy of 140 μJ [12]. THz FELs would be also candidates for light sources with high-repetition-rate and high-power characteristics. In FELIX, THz radiation with maximum micropulse energy up to 50 μJ, tuning range from 1.2 to 100 THz, and repetition rate up to 1 GHz using an FEL oscillator with the electron beam of 45 MeV was reported [6]. Furthermore, experiment of fragmentation of molecules using intracavity setup increased THz pulse energy up to 1 mJ for experiments [13]. Another oscillator-type FEL with maximum micropulse energy of 11 μJ and tuning range from 2 to 12 THz was also reported [14]. Without oscillator FEL, density-modulated electron beams could be THz sources if the frequency of the density modulation is in THz range from a viewpoint of bunching factor [5]. Previously, monochromatic coherent synchrotron radiation was observed at frequency ranging from 0.36 to 0.75 THz using laser modulator [15]. In the laser modulator, chirped pulse beating [16] induced THz slice energy spread modulation in electron bunch with superposed optical pulses for difference frequency generation. The chirped pulse beating in a laser modulator with frequency of 9.2 THz was reported for electron beam of 98 MeV [17]. Optimization of density-modulated electron beam was also reported for electron beam energy of 135 MeV using a laser modulator, linac, and a bunch compressor [18]. Smaller accelerators and laser for high-power THz pulses would have advantages for developments.

In this paper, simulation studies on coherent undulator radiation using electron beam energy ranging from 35 to 50 MeV with modulation frequency up to 10 THz will be reported. Density-modulated electron beam with a bunching factor of ~0.3 based on a laser modulator and bunch compressor is used for THz generation in a helical undulator. THz pulse energy after the undulator of the order on 100 μJ will be discussed.

2. Laser modulator and bunch compressor for THz generation

Figure 1 shows schematic diagram of the proposed THz source in this paper. First, electron beam is generated in a photoinjector driven by a laser and accelerated in a linac for the electron beam energy ranging from 35 to 50 MeV. Second, slice energy spread modulation [18] is given in a laser modulator using THz modulation with a scheme of chirped pulse beating [15-17] or pulse stacker [19]. In the laser modulator, third-harmonic interaction was assumed to ease the choices of undulator parameters. Momentum compaction factor of R_{56} in a chicane-type bunch compressor was optimized for maximizing the bunching factor at a THz frequency which is close to the initial modulation frequency. Third, density-modulated electron beam was matched for coherent undulator radiation with a matching section consisting of two quadrupole magnets (Q1

and Q2 with length of 0.2 m). Finally, coherent undulator radiation in THz undulator was calculated. The lengths of the bunch compressor, matching section, and THz undulator were assumed to be ~7 m, 2 m, and 3 m, respectively

Beam dynamics after the linac was simulated in this paper. Elegant code [20] was used from the exit of the linac to the exit of the matching section for the simulation of beam tracking; Genesis code [21] was used for the coherent undulator radiation in the THz undulator. In the evaluation of the bunching factor, twice of time window with respect to the longitudinal particle distribution was considered in order to improve frequency resolution in the Fourier transform. Fitting results using Gaussian fitting of the frequency spectrum from the Fourier transform was performed for the evaluation of the bunching factor and the central frequency in the THz range.

Table 1 shows parameters in this paper for electron beam energies of 50 and 35 MeV. In each laser modulator, third-harmonic interaction was assumed; fundamental resonant wavelengths in the laser modulators are 2400 nm and 3000 nm for electron beams of 50 and 35 MeV, respectively. Thus, we assumed laser wavelengths of 800 nm and 1000 nm in the master oscillators for the cases of 50 and 35 MeV, respectively. Due to the lower electron beam energy as compared with the previous paper [18], slippage effects were much enhanced and must be properly accounted for in simulations, period in the laser modulator was adjusted from 5 to 20 for electron beam of 50 MeV in order to investigate slippage effects of the laser modulator.

Table 1. Parameters in this paper for electron beam energies of 50 and 35 MeV.

Parameters	Values for 50 MeV	Values for 35 MeV
Electron beam		
Charge (nC)	1	
Bunch length (flattop) (ps)	10	
Intrinsic energy spread	10^{-4}	
Normalized emittance (mm-mrad)	1	
Initial rms beam size (mm)	0.2	
Laser modulator		
Type	Planar type	
Laser wavelength (nm)	800	1000
Rms laser spot size (mm)	0.5	
Amplitude modulation frequency (THz)	2 - 10	
Undulator period (cm)	2.5	
Period number	5, 10, 20	10
Undulator parameter	1.30	0.50
Undulator peak field (T)	0.555	0.215
THz undulator		
Type	Helical type	
Undulator period (cm)	10	
Period number, N_w	30	
Undulator parametor, K_w	5.2 - 2.1	3.7 – 1.3

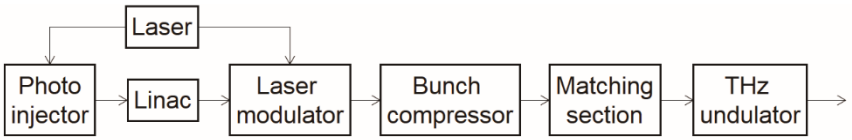

Fig. 1. Schematic diagram of the proposed intense THz source driven by a compact accelerator of 35 to 50 MeV.

3. Bunching factor and slippage effects in laser modulator

To obtain high bunching factor, Elegant tracking simulation was performed from the linac exit to the bunch compressor exit.

Figure 2 shows bunching factor at the exit of the bunch compressor as a function of momentum compaction factor, R_{56}, and slippage effects. The laser power and period in the laser modulator were set to 100 MW and 20, respectively, in Fig. 2 (a) and Fig. 2 (b). Electron beam energy and charge were set to 50 MeV and 1 nC, respectively. Initial modulation frequency of slice energy spread was adjusted from 2 to 6 THz. Lower bunching factor was calculated at initial modulation frequency of 6 THz as compared with the case of 2 THz after optimization of R_{56} as shown in Fig. 2 (a). Relative modulation depth, $0 < A < 1$, given by the laser modulator affects bunching factor after the bunch compressor. If we assume negligible slippage in the laser modulator, bunching factor, b_1, at the fundamental modulation frequency for a Gaussian slice energy spread modulation [18] can be expressed as

$$b_1 \approx \frac{0.58}{2}\left[\exp\left(-\frac{k_0^2 R_{56}^2 \bar{\sigma}^2 (1-0.85A)^2}{2}\right) - \exp\left(-\frac{k_0^2 R_{56}^2 \bar{\sigma}^2 (1+0.85A)^2}{2}\right)\right], \quad (1)$$

where k_0 is the fundamental modulation wave number, and $\bar{\sigma}$ is the average rms slice energy spread after the laser modulator. Larger modulation depth helps larger bunching factor at a condition of $|k_0 R_{56}\bar{\sigma}| \approx \sqrt{2 + 0.5A^2}$ according to Eq. (1). The relative modulation depths, A, after the laser modulator were 0.87, 0.62, and 0.24 at initial modulation frequencies of 2, 4, and 6 THz, respectively, due to slippage effects. The bunching factor as a function of a normalized quantity of $|k_0 R_{56}\bar{\sigma}|$ and theoretical estimations of curves using Eq. (1) were shown in Fig 2 (b). However, discrepancies in the maximum of the bunching factor were observed between the simulation results and theoretical estimations due to the consideration of distribution of slice energy modulation. Maximized bunching factor of ~0.4 was reported in case of slice energy distribution for "double-horn" profile at $|k_0 R_{56}\bar{\sigma}| \approx 1.75$ [18]. Higher bunching factor would be obtained in the cases of initial modulation frequency of 2 and 4 THz due to the "double-horn" profile as compared with the theoretical estimation. And similar conditions of $|k_0 R_{56}\bar{\sigma}| \approx 1.5$ were needed of for maximizing bunching factor in this paper.

To check the slippage effects, laser modulator period was reduced as shown in Fig. 2 (c). The laser power and period in the laser modulator were set to 100 MW and 10, respectively. Decreasing the slippage in the laser modulator with less periods increased

bunching factor at 6 THz. Larger momentum compaction factor of -R_{56} was required for maximizing the bunching factor as compared with Fig. 2 (a). According to Eq. (1), the higher bunching factor can be obtained by maintaining the quantity of $|k_0 R_{56} \bar{\sigma}|$. Short laser modulator decreases the slice energy spread, $\bar{\sigma}$, however, larger momentum compaction factor could maintains the value of $|k_0 R_{56} \bar{\sigma}|$.

The modulation depth depending on slippage effects in the laser modulator was considered because the longer slippage leads to less overlapping between the laser and electron beam. Periods in time for modulation frequencies of 2 and 6 THz correspond to 500 and 167 fs, respectively. Laser modulator used third-harmonic interaction and fundamental wavelength of the laser modulator was 2400 nm, i.e., slippage of 8 fs/period. If we assume a laser modulator of 20 periods, the slippage results in 160 fs which is similar to one period of 6 THz. Thus, modulation depth was decreased in case of laser modulator of 20 periods and bunching factor was decreased at initial modulation frequency of 6 THz.

To maintain higher bunching factor, optimization of both laser modulator period and laser power are essential for appropriate modulation depth. Figure 3 shows bunching factor as function of central frequency for four different laser powers. Central frequency of the maximum of bunching factor was controlled by the initial modulation frequency ranging from 2 to 10 THz in the laser modulator. Three cases of laser modulator periods of 20, 10, and 5 are shown. The maximum bunching factor of 0.11 was calculated at central frequency of ~6 THz with laser modulator period of 20 even if the laser peak power was increased up to 1000 MW as shown in Fig. 3 (a). When the laser power and period in the laser modulator were set to 100 MW and 10, respectively, bunching factor of 0.31 was obtained at ~6 THz due to the reduced slippage as shown in Fig. 3 (b). However, when the laser power and period in the laser modulator were set to 100 MW and 5, respectively, bunching factor of 0.22 was obtained at ~6 THz due to less modulation depth as shown in Fig. 3 (c). The best conditions for high bunching factor were the laser power of 1000 MW and period of 5 because less slippage and larger modulation depth could be obtained in this simulation. The best conditions also improved the bunching factor at other frequencies in addition to the case of ~6 THz.

For the coherent undulator radiation, we focus on the conditions of laser peak power of 100 MW and period of 10 which lead to bunching factor of 0.31 at 5.9 TH. The small difference between the initial modulation frequency and central frequency is due to the electron bunch chirping in the tracking simulation from the laser modulator to the exit of the bunch compressor.

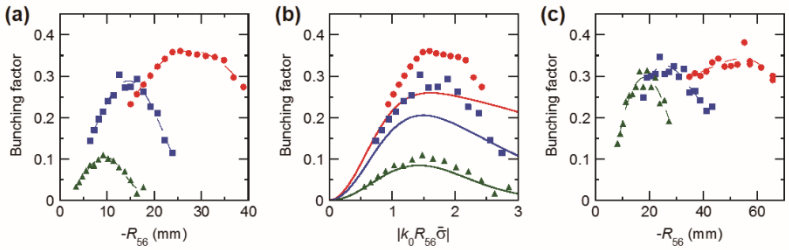

Fig. 2. (a) and (c) Bunching factor as a function of momentum compaction factor, -R_{56}. (b) Bunching factor and theoretical estimation as a function of $|k_0 R_{56} \bar{\sigma}|$; curves are theoretical estimation using Eq. (1) with conditions of A = 0.87, 0.62, and 0.24 from the top. In (a) and (b), laser modulator period was 20. In (c), laser modulator period was 10. Results for three different initial modulation frequencies were shown for 2 (circle), 4 (rectangle), and 6 (triangle) THz. Laser power was fixed to 100 MW.

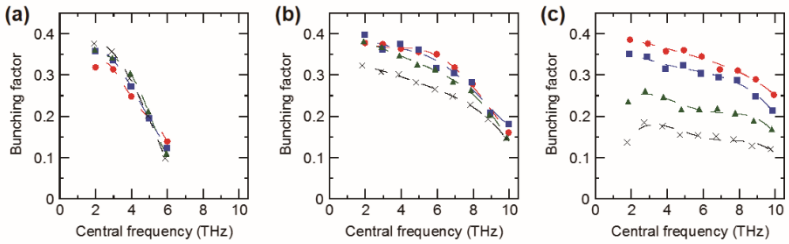

Fig. 3. Maximized bunching factor as a function of central frequency. The results with conditions for laser modulator period of (a) 20, (b) 10, and (c) 5, respectively, were shown. Bunching factor for four different laser powers were shown for 1000 (circle), 400 (rectangle), 100 (triangle), and 40 (cross) MW.

4. FEL simulation for coherent undulator radiation

Coherent undulator radiation using the density modulated electron beam and helical undulator were considered for the estimation of THz pulse energy using analytical estimation. Genesis code was also used for THz undulator simulation with input of beam distribution after the matching section to take into account the FEL interaction. In the matching section, two quadrupole magnets of Q1 and Q2 were used. Electron beam with energy of 50 MeV, charge of 1 nC, and bunching factor of 0.31 at 5.9 THz was considered. Tunable THz frequency and pulse energy from the undulator was studied by changing the initial modulation frequency and undulator parameter of the helical undulator.

4.1. *Estimation of THz power and pulse energy*

In the limit of strong radiation diffraction and assuming no FEL interaction, radiation pulse power, W_0, [22] using a density-modulated electron beam is expressed as

$$W_0 = W_b \left[\frac{\pi^2 a_{in}^2}{2} \right] \left[\frac{I}{\gamma I_A} \right] \left[\frac{K_w^2}{1+K_w^2} \right] N_w , \quad (2)$$

where W_b is the total power of electron beam, $0 < a_{in} < 1$ is the relative current oscillation amplitude in the time domain, I is the beam peak current, I_A is the Alfven current, K_w is the undulator parameter, and N_w is the undulator period. Here we focus on THz radiation at 6 THz with a helical undulator that has a period length of 10 cm, period number N_w of 30, and K_w of 2.9 for the radiation wavelength of 50 μm. If we assume the total power of electron beam, W_b, as 5 GW based on energy of 50 MeV, charge of 1 nC, bunch length of 10 ps, and beam current, I, of 100 A, THz pulse power, W_0, can be estimated to be 14 MW at $a_{in} = 2b_1 = 0.6$ which corresponds to THz pulse energy of 140 μJ at a bunch length of 10 ps. Thus, the THz pulse energy of the order on 100 μJ at 6 THz was estimated for this density-modulated electron beam using the analytical estimation according to Eq. (2).

4.2. *Optimization of matching section and tunable frequency*

The matching section using the two quadrupole magnets of Q1 and Q2 affected not only beam parameters before the helical undulator but also THz pulse energy at the exit of the undulator. The laser power and period in the laser modulator were fixed to 100 MW and 10, respectively.

Figure 4 shows beam parameters before the undulator and THz pulse energy at the exit of the undulator at a central frequency of 5.9 THz. Figure 4 (a) and Figure 4 (b) show beam sizes in x and y, respectively, as functions of two magnetic fields of Q1 and Q2. The conditions for small beam size in x differed from the conditions for small beam size in y before the undulator. Bunching factor was also changed slightly in these ranges of Q1 and Q2 as shown in Fig. 4 (c). Figure 4 (d) shows THz pulse energy at the exit of the helical undulator as functions of magnetic fields of Q1 and Q2. The undulator parameter, K_w, period length, and period number, N_w, were 2.9, 10 cm, and 30, respectively. The length of the undulator was 3 m. As expected with the beam parameters before the undulator, higher THz pulse energy was obtained with conditions for the higher bunching factor although there would be also effects of the beam sizes in x and y. The maximized THz pulse energy was obtained as 570 μJ at the exit of the undulator with Q1/Q2 of -6/9 m^{-2}. The undulator parameter was also optimized for maximizing THz pulse energy practically. Due to the very strong natural focusing of the undulator magnetic field, the matching is not perfect in all quad settings.

Figure 5 shows comparison between the matched (or better matched) and unmatched conditions. The matched and unmatched conditions are Q1/Q2 of -6/9 and -6/12 m^{-2}, respectively. The THz pulse energies at the matched and unmatched conditions were 570 and 150 μJ after 3-m of helical undulator, respectively, as shown in Fig. 5 (a). For the matched condition, THz pulse energy was higher than the analytical estimation using Eq. (2). Bunching factor as a function of longitudinal position was shown in Fig. 5 (b). The matched condition increased bunching factor from 0.30 to 0.75 although the unmatched condition resulted in bunching factor ranging from 0.24 to 0.40. Thus, the increasing bunching factor explained the higher simulated radiation pulse energies than the analytical estimations. The analytical estimation agreed to the energy evolution of the

matched condition at the longitudinal position of z<1 m when the FEL interaction is negligible. The rms electron beam sizes in x and y through the undulator at the matched and unmatched conditions were shown in Fig. 5 (c). The matched condition resulted in smaller electron beam size, i.e., averaged size of 0.31 mm in the FEL, as compared with the unmatched condition, i.e., averaged size of 1.1 mm. Small electron beam size would help increasing the bunching factor. For the matched condition, THz transverse profile at the exit of the helical undulator was shown in Fig. 5 (d). The transverse size of the THz pulse had a size of ~3 mm in FWHM. The time profile of the THz pulse had a length of 8.9 ps in FWHM.

Figure 6 shows THz pulse energy as a function of the central frequency. The central frequency was changed by the initial modulation frequency in the laser modulator. The undulator parameter was changed from 5.2 to 2.1 for optimizing the THz pulse energy at central frequency ranging from 1.8 to 9.8 THz. The maximum THz energy was 750 μJ at 3.9 THz with bunching factor of 0.35. The THz energy was 90 μJ at 9.9 THz. Thus, the THz energy yield of the order on 100 μJ was indicated from the analytical estimation and Genesis simulation. The laser pulse energy at the wavelength of 800 nm in the modulator corresponds to 1 mJ if we assume the laser pulse width and power of 10 ps and 100 MW, respectively. The results mean THz generation of ~100 μJ from the 1-mJ laser energy in this case although it is hard to discuss the conversion efficiency from laser to THz energy due to the combination of laser modulator and relativistic electron beam. Thus, THz source based on laser modulator and relativistic electron beam could be one of the very efficient schemes for high-power THz pulses via coherent undulator radiation using density modulated beam.

In passing, we would like to comment on the validity of Genesis simulations. First, we assume no vacuum pipe in the FEL simulations although the existence of the vacuum pipe in the undulator section may help guide the THz radiation to overcome the diffraction. Secondly, the FEL gain length (estimated from the 3D FEL theory) and the Rayleigh length of the radiation at 6 THz were both several undulator periods so that the undulator-averaging model of the Genesis simulation is valid at relatively high THz frequencies. At lower THz frequencies such as 2-4 THz, both the FEL gain length and the Rayleigh length may become comparable to the undulator period, so the Genesis code may not be sufficient to simulate the radiation generation process and hence we take the pulse energy between 2-4 THz in Fig. 6 as very rough estimations.

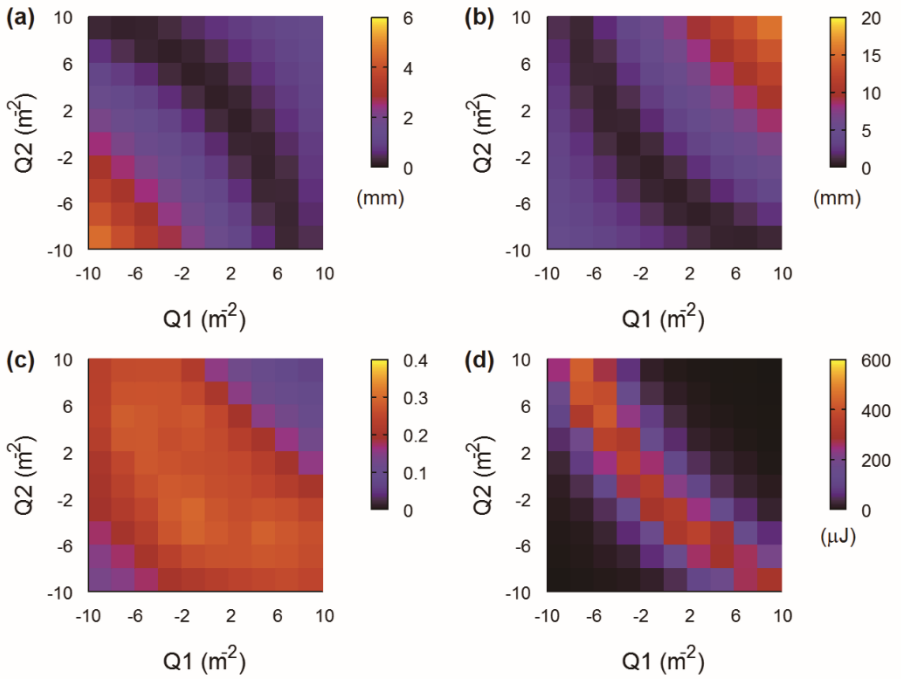

Fig. 4. (a) Beam size in x, (b) beam size in y, and (c) bunching factor at a central frequency of 5.9 THz before the undulator. (d) THz pulse energy at the exit of the undulator at 5.9 THz. The maximized THz pulse energy was obtained as 570 μJ at the matching section with Q1/Q2 of -6/9 m^{-2}.

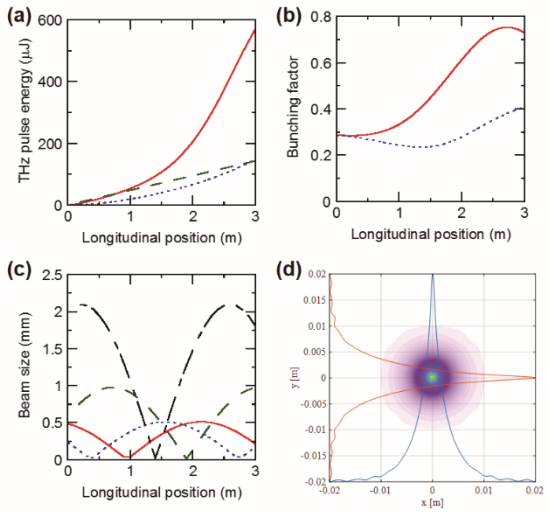

Fig. 5. (a) THz pulse energy as a function of longitudinal position. Solid and dotted lines denote matched and unmatched conditions, respectively. Dashed line denotes the analytical estimation using Eq. (2). (b) Bunching factor as a function of longitudinal position. Solid and dotted lines denote matched and unmatched conditions, respectively. (c) Rms electron beam sizes as a function of longitudinal position. Solid and dotted lines denote beam size in x and y, respectively, at matched condition. Dashed and dash-dot lines denote beam size in x and

y, respectively, at unmatched condition. (d) THz transverse profile at the exit of the helical undulator at matched condition.

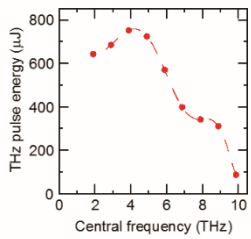

Fig. 6. THz pulse energy as a function of the central frequency. The undulator parameter was changed from 5.2 to 2.1 for optimizing the THz pulse energy at central frequency ranging from 1.8 to 9.8 THz.

5. Coherent undulator radiation using electron beam of 35 MeV

Smaller accelerator would give more flexibility for development and experiment in THz generation and applications. Coherent undulator radiation using electron beam of 35 MeV [23] was considered. Figure 7 shows the simulation results for coherent undulator radiation using electron beam of 35 MeV. Third harmonic interaction was also used in the laser modulator of 10 periods; fundamental resonant wavelength and the laser wavelength are 3000 and 1000 nm, respectively, as shown in Table 1. Figure 7 (a) shows the bunching factor as a function of central frequency. The central frequency was controlled by the initial modulation frequency ranging from 2 to 10 THz. However, bunching factor was lower as compared with the case of 50 MeV in Fig. 3 (b) due to longer slippage. Figure 7 (b) shows the THz pulse energy as a function of the central frequency. Laser power was set to 1000 MW. Due to the lower beam power, W_b, and bunching factor, the THz pulse energy was lower as compared with the case of 50 MeV. However, the THz pulse energies of 540, 390, 29 μJ were obtained at central frequencies of 2.8, 5.8, and 9.8 THz, respectively. These THz pulse energies would be also useful for the study of nonlinear effect and structural control in material science.

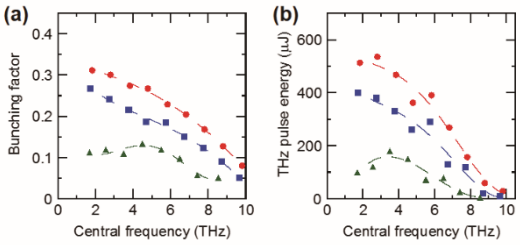

Fig. 7. (a) Bunching factor as a function of central frequency. (b) THz pulse energy as a function of the central frequency. Laser power was set to 1000 MW. Results for three different laser powers in the laser modulator were shown for 1000 (circle), 400 (rectangle), and 100 (triangle) MW.

6. Summary

In summary, simulation studies on the intense THz source based on laser modulator and bunch compressor with electron beam ranging from 35 to 50 MeV were performed for coherent radiation in a helical undulator of 3 m in length. Bunch length and charge of the electron beam were set to 10 ps and 1 nC, respectively. Slippage in the laser modulator was investigated and bunching factor of 0.31 was simulated at 5.9 THz with the laser power of 100 MW and the laser modulator of 10 period. THz pulse energies were obtained as 750, 570, and 90 μJ at 3.9, 5.9, and 9.9 THz, respectively, using electron beam of 50 MeV. Optimization of a matching section increased bunching factor in the undulator. Feasibility of coherent undulator radiation using electron beam of 35 MeV was also proposed. THz pulse energies were obtained as 540, 390, and 29 μJ at 2.8, 5.8, and 9.8 THz, respectively, in the case of 35 MeV. Both the laser and the accelerator can operate at very high-repetition rate. For example, at 100 kHz, the laser average power for the studied cases is 100 W, and the average electron beam power is on the order of kW. Thus, the proposed intense THz radiation can be a high-repetition rate stand-alone source or as a part of the integrated facility in a high-repetition rate FEL such as the European XFEL [24] or the LCLS-II [25].

Acknowledgments

We thank useful discussions with B. Garcia, T. Maxwell, and R. W. Schoenlein (SLAC National Accelerator Laboratory). This work is supported by U.S. Department of Energy Contract No. DE-AC02-76SF00515 and Program for Advancing Strategic International Networks to Accelerate the Circulation of Talented Researchers from Japan Society for the Promotion of Science (JSPS) for "Global Networking on Molecular Technology Research".

References

1. W. Ackermann, G. Asova, V. Ayvazyan, A. Azima, N. Baboi, J. Bähr, V. Balandin, B. Beutner, A. Brandt, A. Bolzmann *et al.*, Operation of a free-electron laser from the extreme ultraviolet to the water window, *Nat. Photonics* **1**, 336 (2007).
2. P. Emma, R. Akre, J. Arthur, R. Bionta, C. Bostedt, J. Bozek, A. Brachmann, P. Bucksbaum, R. Coffee, F.-J. Decker *et al.*, First lasing and operation of an ångstrom-wavelength free-electron laser, *Nat. Photonics* **4**, 641 (2010).
3. T. Ishikawa, H. Aoyagi, T. Asaka, Y. Asano, N. Azumi, T. Bizen, H. Ego, K. Fukami, T. Fukui, Y. Furukawa *et al.*, A compact X-ray free-electron laser emitting in the sub-ångström region, *Nat. Photonics* **6**, 540 (2012).
4. E. Allaria, R. Appio, L. Badano, W.A. Barletta, S. Bassanese, S.G. Biedron, A. Borga, E. Busetto, D. Castronovo, P. Cinquegrana *et al.*, Highly coherent and stable

pulses from the FERMI seeded free-electron laser in the extreme ultraviolet, *Nat. Photonics* **6**, 699 (2012).

5. G. Wang *et al.*, Commissioning status of the Dalian Coherent Light Source, WEPAB058, in *Proc. IPAC2017*, (Copenhagen, Denmark, 2017).
6. A. F. G. van der Meer, FELs, nice toys or efficient tools?, *Nucl. Instrum. Meth. A* **528**, 8 (2004).
7. Frontiers of THz Science, 5-6 September, 2012, SLAC National Accelerator Laboratory, https://portal.slac.stanford.edu/sites/conf_public/THz_2012_09/Pages/default.aspx.
8. M. Jewariya, M. Nagai, K. Tanaka, Ladder Climbing on the Anharmonic Intermolecular Potential in an Amino Acid Microcrystal via an Intense Monocycle Terahertz Pulse, *Phys. Rev. Lett.* **105**, 203003 (2010).
9. H. Hirori, K. Shinokita, M. Shirai, S. Tani, Y. Kadoya, K. Tanaka, Extraordinary carrier multiplication gated by a picosecond electric field pulse, *Nat. Commun.* **2**, 594 (2011).
10. C. Vicario, B. Monoszlai, C. P. Hauri, GV/m Single-Cycle Terahertz Fields from a Laser-Driven Large-Size Partitioned Organic Crystal, *Phys. Rev. Lett.* **112**, 213901 (2014).
11. M. Shalaby, C. Vicario, C. P. Hauri, High-performing nonlinear visualization of terahertz radiation on a silicon charge-coupled device, *Nat. Commun.* **6**, 8439 (2015).
12. D. Daranciang, J. Goodfellow, M. Fuchs, H. Wen, S. Ghimire, D. A. Reis, H. Loos, A. S. Fisher, A. M. Lindenberg, Single-cycle terahertz pulses with >0.2 V/Å field amplitudes via coherent transition radiation, *Appl. Phys. Lett.* **99**, 141117 (2011).
13. J. M. Bakker, V. J. F. Lapoutre, B. Redlich, J. Oomens, B. G. Sartakov, A. Fielicke, G. von Helden, G. Meijer, A. F. G. van der Meer, Intensity-resolved IR multiple photon ionization and fragmentation of C_{60}, *J. Chem. Phys.* **132**, 074305 (2010).
14. K. Kawase, R. Kato, A. Irizawa, M. Fujimoto, S. Kashiwagi, S. Yamamoto, F. Kamitsukasa, H. Osumi, M. Yaguchi, A. Tokuchi *et al.*, The high-power operation of a terahertz free-electron laser based on a normal conducting RF linac using beam conditioning, *Nucl. Instrum. Meth. A* **726**, 96 (2013).
15. S. Bielawski, C. Evain, T. Hara, M. Hosaka, M. Katoh, S. Kimura, A. Mochihashi, M. Shimada, C. Szwaj, T. Takahashi *et al.*, Tunable narrowband terahertz emission from mastered laser–electron beam interaction, *Nat. Phys.* **4**, 390 (2008)
16. A. S. Weling, B. B. Hu, N. M. Froberg, D. H. Auston, Generation of tunable narrow‐band THz radiation from large aperture photoconducting antennas, *Appl. Phys. Lett.* **64**, 137 (1994).
17. E. Roussel, E. Ferrari, E. Allaria, G. Penco, S. Di Mitri, M. Veronese, M. Danailov, D. Gauthier, L. Giannessi, Multicolor High-Gain Free-Electron Laser Driven by Seeded Microbunching Instability, *Phys. Rev. Lett.* **115**, 214801 (2015).

18. Z. Zhang, L. Yan, Y. Du, W. Huang, C. Tang, Z. Huang, Generation of high-power, tunable terahertz radiation from laser interaction with a relativistic electron beam, *Phys. Rev. Accel. Beams* **20**, 050701 (2017).
19. L.-X. Yan, J.-F. Hua, Y.-C. Du, Y.-F. Huang, Y. You, D. Wang, W.-H. Huang, C.-X. Tang, UV pulse trains by α-BBO crystal stacking for the production of THz-rap-rate electron bunches, *J. Plasma Phys.* **78**, 429 (2012).
20. M. Borland, elegant: A Flexible SDDS-Compliant Code for Accelerator Simulation, Advanced Photon Source LS-287, September 2000.
21. S. Reiche, Numerical Studies for a Single Pass High Gain Free-Electron Laser, DESY print, DESY-THESIS-2000-012 (2000).
22. E. L. Saldin, E. A. Schneidmiller, M. V. Yurkov, A simple method for the determination of the structure of ultrashort relativistic electron bunches, *Nucl. Instrum. Meth. A* **539**, 499 (2005).
23. I. Nozawa, K. Kan, J. Yang, A. Ogata, T. Kondoh, M. Gohdo, K. Norizawa, H. Kobayashi, H. Shibata, S. Gonda *et al.*, Measurement of <20 fs bunch length using coherent transition radiation, *Phys. Rev. ST Accel. Beams* **17**, 072803 (2014).
24. W. Decking, H. Weise *et al.*, Comissioning of the European XFEL accelerator, MOXAA1, in *Proc. IPAC2017*, (Copenhagen, Denmark, 2017).
25. LCLS-II Conceptual Design Report, LCLSII-1.1-DR-0001-R0, 2013.